Contribution of Dissipative Heating to the Intensity-Dependence of

2	Tropical Cyclone Intensification
3	Yuqing Wang ^a , Jing Xu ^b , and Zhe-Min Tan ^c
4	^a International Pacific Research Center and Department of Atmospheric Sciences, University
5	of Hawaii at Mānoa, Honolulu, HI 96822
6	^b State Key Laboratory of Severe Weather, Chinese Academy of Meteorological Sciences,
7	China Meteorological Administration, Beijing 100081, China
8	^c Key Laboratory of Mesoscale Severe Weather/MOE, and School of the Atmospheric
9	Sciences, Nanjing University, Nanjing, China

- 10 <u>January 12, 2022 (submitted)</u>
- 11 <u>April 20, 2022 (revised)</u>
- 12 Dateline

1

- 13 Submitted to *Journal of the Atmospheric Sciences*
- 14 Corresponding author: Yuqing Wang, yuqing@hawaii.edu

15 ABSTRACT

Previous studies have demonstrated the contribution of dissipative heating (DH) to the maximum potential intensity (MPI) of tropical cyclones (TCs). Since DH is a function of near-surface wind speed and thus TC intensity, a natural question arises as to whether DH contributes to the intensity-dependence of TC potential intensification rate (PIR). To address this issue, an attempt has been made to include DH in a recently developed time-dependent theory of TC intensification. With this addition, the theory predicts a shift of the maximum PIR towards the higher intensity side, which is consistent with the intensity-dependence of TC intensification rate in observed strong TCs. Since the theory without DH predicts a dependence of TC PIR on the square of the MPI, the inclusion of DH results in an even higher PIR for strong TCs. Considering the projected increase in TC MPI under global warming, the theoretical work implies that as the climate continues to warm, TCs may intensify more rapidly. This may not only make the TC intensity forecasting more difficult, but also may increase the threats of TCs to the coastal populations if TCs intensify more rapidly just before they make landfall.

SIGNIFICANCE STATEMENT

Previous studies have demonstrated that dissipative heating (DH) can significantly contribute to the maximum potential intensity (MPI) that a tropical cyclone (TC) can achieve given favorable environmental thermodynamic conditions of the atmosphere and the underlying ocean. Here we show that because DH is a function of near-surface wind speed and thus TC intensity, DH can also significantly contribute to the intensity-dependence of TC potential intensification rate (PIR). This has been demonstrated by introducing DH into a recently developed time-dependent theory of TC intensification. With DH the theory predicts a shift of the maximum PIR towards the higher intensity side as observed in strong TCs. Therefore, as the climate continues to warm, TCs may intensify more rapidly and become stronger.

1. Introduction

Considering energy conservation, the viscous dissipation of kinetic energy due to surface friction can be considered as an internal heat source to the thermodynamic equation of motion. Such a heat source to the thermodynamic energy is often termed dissipative heating (DH). Although DH is relatively small compared to the direct surface heat flux under normal

near-surface wind conditions (e.g., less than 10 m s 1) over the ocean, it can be a considerable
energy source to the development and maintenance of tropical cyclones (TCs) because DH
roughly increases with the cube of the near-surface wind speed. Bister and Emanuel (1998,
hereafter BE98) first introduced DH into the theoretical maximum potential intensity
(EMPI) ¹ of TCs developed by Emanuel (1986, 1997). They showed that the inclusion of DH
due to surface friction in TC surface layer could lead to an increase in the theoretical EMPI in
terms of the near-surface wind speed by approximately 20%. This was confirmed by
idealized numerical simulations using two different axisymmetric models of different
complexities. Their results showed that both the intensification rate and the quasi-steady
intensity of the simulated TCs increased significantly with the DH included. They therefore
advocated that the DH should be considered in the thermodynamic equation of models used
to simulate and predict intensity of TCs.

Zhang and Altshuler (1999) included DH in a simulation of Hurricane Andrew (1992) using a high-resolution mesoscale model and showed that the effect of DH on the simulated storm intensity was not significant until the surface wind speed exceeds 65 m s⁻¹ and the simulated storm intensity in terms of maximum near-surface wind speed increased by only 10% at the most intense stage compared with that in the simulation without DH. They found that the inclusion of DH also led to a decrease in surface sensible heat flux, which partially offset the DH effect. Jin et al. (2007) examined the impact of DH on the TC intensity forecasts for 18 different storms using the U.S. Navy's operational Coupled Ocean—Atmosphere Mesoscale Prediction System (COAMPS). They found that the inclusion of DH in the model significantly improved the intensity forecasts, although there was no significant change for the track forecasts. They also compared the surface-only DH due to surface friction as in BE98 and the DH related to the turbulent kinetic energy dissipation rate and found that the former was often considerably larger than the latter. More recently, Fox and

¹The MPI is defined as the upper bound of the intensity that a TC can reach under favorable environmental thermodynamic conditions. In this study, the MPI without the inclusion of DH developed by Emanuel (1986, 1997) is termed as EMPI.

- 72 Judt (2018) performed a numerical study on the extremely rapid intensification of Hurricane
- Patricia (2015). They found that DH was one of the key factors to the realistic simulation of
- 74 the Patricia's intensity evolution although the storm intensity was overpredicted without the
- ocean coupling, suggesting that DH could be important in extremely intense TCs in nature.
- 76 The increased maximum intensity of simulated TCs in numerical simulations with the
- inclusion of DH is also reported in some other studies (e.g., Wang 2001; Zeng et al. 2010;
- 78 Cheng et al. 2012).
- Kieu (2015) reexamined the hypothesis of DH in BE98 by analyzing the integral energy
- 80 equation for the atmospheric domain that encloses all the TC Carnot legs. He indicated that
- 81 within the atmospheric surface layer, the DH comes at the expense of reduced internal kinetic
- 82 energy in the boundary layer, which was not included in BE98. He also suggested that not all
- the work done by surface friction is converted to DH to fuel the TC and about 10-30% of the
- work could be transferred to the ocean surface waves and ocean mixing layer. Given
- uncertainties in how the DH is distributed in the atmospheric surface layer and is exchanged
- with the ambient environment, Kieu (2015) recommended that the DH in the TC surface
- layer could be effectively included in the bulk enthalpy flux parametrization instead of being
- 88 considered as an independent heat source as in BE98. Following this suggestion, Edwards
- 89 (2019) considered the total (thermal and kinetic) energy flux at the air-sea interface and
- 90 modified the bulk surface heat flux formula to include the impact of frictional dissipation
- 91 within the atmospheric surface layer. With such a modification, he reformulated the MPI of
- 92 BE98 and showed a reduced increase of the MPI by DH from 22.5% to 16.6%. He explained
- 93 this as a result of the reduced surface sensible heat flux due to the inclusion of DH, which
- acts to reduce the air-sea temperature difference by warming the surface air.
- In addition to the theoretical and modeling studies focusing on the possible impact of DH
- on TC intensity, some studies have attempted to estimate DH based on observations. Using
- 97 low-level in-situ aircraft observations, Zhang (2010) estimated DH in the hurricane boundary
- 98 layer in the North Atlantic and found that the DH rate estimated with the integrated
- 99 turbulence kinetic energy dissipation rate in the surface layer using the turbulent spectra
- method was considerably smaller than that estimated with the product of the surface drag
- 101 coefficient and the cube of the surface wind speed proposed by BE98. This result is supported
- in a more recent study by Smith et al. (2019), who used the high-resolution ship
- measurements to estimate DH in the non-hurricane atmospheric surface layer. Several other
- studies estimated DH using data from portable weather stations (Zhang et al. 2011) or towers

(Ming and Zhang 2018; Zhou et al. 2022) in landfalling TCs and also reported the
overestimation of DH using the earlier bulk formula as in BE98 and other numerical models.
Note that Ming and Zhang (2018) found that the overestimation was generally less over land
than over shallow waters. This seems to suggest that part of turbulent dissipation was likely
transferred to the underlying ocean as pointed out by Kieu (2015).

Some issues remain regarding the treatment of DH in TCs as mentioned above. For example, Kieu (2015) questioned whether the DH estimated in the atmospheric surface layer is physically consistent with the assumptions in the MPI theory in BE98. Both Makarieva et al. (2010) and Edwards (2019) argued that whether DH in the atmospheric surface layer may reduce the external heat input, namely the surface heat flux. Nevertheless, some agreements are reached, including that (1) not all the work done by surface friction is converted to DH in the atmospheric surface layer to fuel the TC system as previously hypothesized because part of it could be transferred to the ocean surface waves and ocean mixing layer; and (2) the estimation of DH using the bulk formula might overestimate the DH to some extent. One of the best ways to address these issues is to include DH in high-resolution numerical models that treat the turbulent kinetic energy dissipation rate as one of the prognostic variables, such as in the so-called E- ϵ turbulent closure scheme recently implemented into the Weather Research and Forecasting (WRF) model (Zhang et al. 2020).

Instead of performing high-resolution numerical modeling, we introduce the effect of DH in the atmospheric surface layer into a recently developed time-dependent theory of TC intensification (Wang et al. 2021a, b). We will show that the inclusion of DH makes the theoretically estimated potential intensification rate (PIR)² more consistent with observations in terms of the dependence of the intensification rate on TC intensity and the estimated PIR,

²Potential intensification rate (PIR) is defined as the possible intensification rate a perfect TC can reach under all favorable environmental dynamic and thermodynamic conditions. Note that the PIR is a function of TC intensity and for a given intensity, there exists a PIR. The PIR often reaches a peak in some immediate intensity, which we refer to the maximum PIR (MPIR). See Xu and Wang (2022) for more details on these definitions. Note that in our discussion, because the current theory does not include any environmental effects, the theoretical intensification rate thus is the PIR by definition.

especially for category 5 TCs. The rest of the paper is organized as follows. Section 2
reformulates the theoretical time-dependent TC PIR equation with the DH included. Section
3 provides some calculations to demonstrate the contributions of DH to the time-dependence
of TC PIR and compared with the best-track TC data. Main conclusions are drawn in the last
section.

2. Inclusion of DH in a time-dependent theory of TC intensification

As in Wang et al. (2021a), we start with the tangential wind and entropy budget equations in the axisymmetric slab boundary layer in cylindrical coordinates. Here, we introduce two terms related to frictional dissipation in the atmospheric boundary layer mentioned in section 1, namely the reduced surface heat flux due to the loss of kinetic energy as implied from Eq. (8) in Edwards (2019) and the DH due to frictional dissipation (BE98; Emanuel 2017a). With the two additions, the tangential wind and entropy budget equations in Wang et al. (2021a) are modified to

$$\frac{\partial V_b}{\partial t} + u_b \frac{\partial M_b}{r \partial r} = -\frac{c_D}{h} |\overrightarrow{V}_{10}| V_{10}, \tag{1}$$

$$\frac{\partial s_b}{\partial t} + u_b \frac{\partial s_b}{\partial r} = \frac{\beta}{h} \left[C_k | \overrightarrow{V}_{10}| \left(s_0^* - s_b - \frac{\gamma \delta}{2} \frac{|\overrightarrow{V}_{10}|^2}{T_S} \right) + \gamma C_D \frac{|\overrightarrow{V}_{10}|^3}{T_S} \right], \tag{2}$$

where t is time, r is radius, u and V are radial and tangential wind speeds, respectively, M is the absolute angular momentum ($M = rV + \frac{1}{2}fr^2$, with f being the Coriolis parameter), C_k and C_D are the surface enthalpy exchange coefficient and surface drag coefficient, $|\overrightarrow{V}_{10}|$ and V_{10} are the total wind speed and the tangential wind speed at 10-m height above the sea surface, respectively, s_0^* and s_b are the saturated entropy at the sea surface temperature (SST, T_s) and the air entropy in the well-mixed boundary layer, the parameter β in Eq. (2) describes the effects of subsaturation and/or downdrafts on the mixed layer entropy budget (Emanuel 1997; Gray and Craig 1998; Frisius 2006), δ is a tracking parameter to switch the possible effect of DH on surface heat flux when DH is considered ($1 \ge \gamma > 0$) as recently advocated

by Edwards $(2019)^3$, and γ is the percentage of the viscous frictional dissipation that is converted to internal DH to warm the atmospheric surface layer [and the remaining part $(1-\gamma)$ is transferred to the ocean surface waves and ocean mixing layer, as advocated by Kieu 2015]. All variables with subscript "b" are their vertical means in the slab boundary layer, which has a depth of h. Note that the horizontal diffusions of both tangential wind and entropy in Eqs. (1) and (2) are neglected as in previous theoretical studies of TC MPI and intensification theories (e.g., Emanuel 1986; 1988; 2012; Emanuel and Rotunno 2011; Wang et al. 2021a,b) although they may be important across the eyewall in strong TCs (Emanuel 1997; Rotunno and Bryan 2012; Zhang and Marks 2015).

Since our interest is on TC intensification, we evaluate all terms in Eqs. (1) and (2) following the radius of maximum wind (RMW) near the surface where β is often close to 1.0 (Gray and Craig 1998; Frisius 2006). As in Wang et al. (2021a), we further assume that the TC boundary layer is in thermodynamic quasi-equilibrium, which is well supported by our full-physics model simulations as mentioned in Wang et al. (2021a) and was also assumed in convective parameterization in numerical models to simulate TC development in some previous studies (e.g., Emanuel 1995; Gray and Craig 1998; Frisius 2006). In this case, β can be considered being less than 1.0 during the TC intensification because part of the surface enthalpy flux would contribute to increasing entropy near the RMW. With these assumptions, Eq. (2) becomes

171
$$u_b \frac{\partial s_b}{\partial r} = \frac{\beta}{h} \left[C_k | \overrightarrow{V}_{10}| \left(s_0^* - s_b - \frac{\gamma \delta}{2} \frac{|\overrightarrow{V}_{10}|^2}{T_S} \right) + \gamma C_D \frac{|\overrightarrow{V}_{10}|^3}{T_S} \right],$$
 (3)

 3 Note that the term with δ is considered here because in the theoretical framework we do not explicitly consider the possible reduction of surface heat flux due to the warmed atmospheric surface layer associated with DH, as found in numerical simulations (Zhang and Altshuler 1999; Wang 2001; Jin et al. 2007; Zeng et al. 2010; Edwards 2019) and in nature. This term should not be included in full-physics models in which the warming in the atmospheric surface layer is explicitly resolved if DH is considered. This is why we treat δ as a tracking parameter, which can switch from 0 to 1 or vice versa, together with γ . See further discussions in section 3.

172 Replacing u_b in Eq. (1) from Eq. (3) above gives

173
$$h\frac{\partial V_b}{\partial \tau} = -\frac{\beta}{r_m}\frac{\partial M_b}{\partial r} \left[C_k | \overline{V_{10}}| \left(s_0^* - s_b - \frac{\gamma \delta}{2} \frac{|\overline{V_{10}}|^2}{T_S} \right) + \gamma C_D \frac{|\overline{V_{10}}|^3}{T_S} \right] / \frac{\partial s_b}{\partial r} - C_D | \overline{V_{10}}| V_{10}. \tag{4}$$

- Note that from Eq. (4), we start to use τ instead of t because the budget and all variables
- are now evaluated at and following the RMW as in Wang et al. (2021a). Since the total wind
- speed near the RMW is close to the tangential wind speed, we can simply assume
- 177 $|\overrightarrow{V_{10}}| \approx V_{10} = V_m$. We further assume $V_m = \alpha V_{b,m}$, where α is the reduction factor of the
- depth-averaged boundary layer tangential wind speed to the near-surface tangential wind
- speed at the RMW, which is roughly between 0.7~0.8 (Vickery et al. 2000; Powell et al.
- 180 2003). With these assumptions and approximations, Eq. (4) can be rewritten as

181
$$\frac{\partial V_m}{\partial \tau} = \frac{\alpha}{h} \left[-\frac{\beta}{r_m} \frac{\partial M}{\partial s} \Big|_{b, r_m} \left\langle C_k V_m \left(s_0^* - s_b - \frac{\gamma \delta}{2} \frac{V_m^2}{T_s} \right) \Big|_{r_m} + \gamma C_D \frac{V_m^3}{T_s} \right\rangle - C_D V_m^2 \right]. \tag{5}$$

- Note that $\partial V_m/\partial \tau$ is equivalent to $dV_m/d\tau$ at the RMW. This is because $dV_m/d\tau =$
- 183 $\partial V_m/\partial \tau + \dot{r}_m(\partial V_m/\partial r)$ and $\partial V_m/\partial r = 0$ at the RMW.
- 184 Equation (5) is closed if $\frac{\partial M}{\partial s}\Big|_{h,r}$ can be determined and the dependence of the surface
- enthalpy dis-equilibrium on TC intensity can be given. Here, as in Emanuel (1986) and Wang
- et al. (2021a), we further assume that $\frac{\partial M}{\partial s}\Big|_{h,r}$ can be evaluated at the top of the boundary
- layer $\left(\frac{\partial M}{\partial s}\Big|_{h.r.}\right)$ and treat the TC as an axisymmetric vortex in hydrostatic and gradient wind
- balance and thus in the thermal wind balance in the free atmosphere. Emanuel (1986, 2012)
- assumed that both the moist entropy (s) and M are conserved along streamlines in the eyewall
- ascent above the boundary layer, and thus the s and M surfaces can be considered being
- almost congruent in the free atmosphere. As noticed by Peng et al. (2018), although the
- assumption of moist-neutral ascent in the eyewall is a good approximation for a strong and
- mature TC, it is often not satisfied for weak TCs and for TCs during their early intensification
- stage. Namely, the M and s surfaces may intersect and not be congruent. To consider this,
- Wang et al. (2021a) introduced an *ad-hoc* empirical parameter A' as a measure of the extent
- to which the M surface is parallel to the s surface and modified Eq. (4) of Emanuel (2012)
- into the following equation [see Eq. (14) in Wang et al. (2021a)]

$$\frac{\partial M}{\partial s}\Big|_{b,r_m} \cong \frac{\partial M}{\partial s}\Big|_{h,r_m} = -A' \frac{T_b - T_0}{M_{h,r_m} \left(\frac{1}{r_m^2} - \frac{1}{r_0^2}\right)},$$
(6)

where (r_m, h) means the point through the RMW at the top of the boundary layer, r_0 is a large

200 radius at which the tangential wind following the trajectory of the eyewall ascent in the

outflow layer becomes zero and the air temperature is T_0 , and T_b is the air temperature at $(r_m,$

- 202 h), which is assumed to be the same as the SST without the loss of accuracy (Emanuel 1986,
- 203 2012; Bryan and Rotunno 2009). The *ad-hoc* parameter A' satisfies $0 \le A' \le 1$ since
- $(\partial M/\partial s)_{h,r_m} \le 0$ in TCs and is a function of the TC intensity. It should be close to 1.0 when
- 205 the inner-core convection reaches a nearly moist-neutral state with the M and s surfaces being
- almost congruent, while it is close to zero in the early incipient stage when V_m is close to zero
- and the *M* and *s* surfaces are nearly orthogonal (Peng et al. 2018; Wang et al. 2021a).
- Substituting Eq. (6) into Eq. (5), Eq. (5) becomes

$$\frac{\partial V_m}{\partial \tau} = \frac{\alpha}{h} \left[\frac{\varepsilon A' \beta}{M_{h,r_m} \left(\frac{1}{r_m^2} - \frac{1}{r_0^2} \right)} \langle C_k V_m \left(k_0^* - k_b - \frac{\gamma \delta}{2} V_m^2 \right) \Big|_{r_m} + \gamma C_D V_m^3 \rangle - C_D V_m^2 \right], \tag{7}$$

- where $\varepsilon = \frac{T_S T_0}{T_S}$ is the thermodynamic efficiency (Emanuel 1986), k_0^* and k_b are the
- saturation enthalpy at T_s ($\approx T_b$) and the air enthalpy of the boundary layer at the RMW,
- respectively, with the approximation $T_s(s_0^* s_b) \approx (k_0^* k_B)$ being used as in Emanuel
- 213 (2012). In Eq. (7), $M_{h,r_m} = r_m(V_{h,r_m} + \frac{1}{2}fr_m)$, where V_{h,r_m} is the maximum gradient wind
- speed at the top of the boundary layer, and by definition $V_m = 0$ at r_0 , we have $M_{h,r_m} = 0$
- 215 $\frac{1}{2}fr_0^2$, or $\frac{1}{r_0^2} = \frac{f}{2M_{h,r_m}}$ should be satisfied. If we further assume $V_m = V_{h,r_m}$, Eq. (7) can be
- 216 simplified to

$$\frac{\partial V_m}{\partial \tau} = \frac{\alpha C_D}{h} \left\{ A V_{EMPI}^2 - \left[1 - \gamma A \varepsilon \left(1 - \frac{\delta C_k}{2C_D} \right) \right] V_m^2 \right\}, \tag{8}$$

- where $A = \beta A'$ as in Wang et al. (2021a), and the surface-wind-based EMPI without
- considering the effect of DH is given (Emanuel 1997) by

$$V_{EMPI} = \sqrt{\frac{c_k}{c_D} \varepsilon(k_0^* - k_b)|_{r_m}}.$$
 (9)

- Note that C_D should be treated consistently in Eqs. (8) and (9). This means that the
- theoretical intensification rate does not increase linearly with increasing C_D but increases with
- 223 increasing C_k significantly. The weak dependence of the TC intensification rate on C_D was
- also found in full-physics high-resolution simulations by Li and Wang (2021). Note also that
- because of the dependence of surface saturation enthalpy on surface air pressure, the EMPI in

Eq. (9) also depends on the surface air pressure at the RMW and thus the TC intensity. This dependence can considerably increase the calculated EMPI, which is included in the standard algorithm of Bister and Emanuel (2002). Note that theoretically the surface saturation enthalpy in Eq. (9) should be calculated using a time-dependent surface air pressure at the RMW for use in Eq. (8). However, results from our preliminary tests show that the use of the surface air pressure of the steady-state solution and the use of a time-dependent surface air pressure at the RMW produce quite small discrepancies in the time-dependent solution of Eq. (8) (not shown). Considering the simplicity of the theoretical model, the small discrepancies induced by such an approximation is acceptable and can thus be ignored. Therefore, the surface air pressure in the steady-state solution is used in calculating the surface saturation enthalpy at the RMW in Eq. (9) in our practical applications discussed in section 3.

Before quantifying the effect of DH on the TC PIR in the dynamical framework outlined above, it is our interest to examine the maximum intensity of the TC, namely the steady-state solution of Eq. (8), and compared it with that in the relevant previous studies. To do so, we assume that the TC reaches the maximum intensity with a zero-intensification rate, namely $\frac{\partial V_m}{\partial \tau} = 0$. In this steady-state stage, the moist neutral eyewall ascent can be assumed, and the M and s surfaces can be considered being congruent. We can thus assume $A \approx 1$. From Eq. (8), we can get the steady-state intensity below

$$V_{max} = \frac{V_{EMPI}}{\sqrt{1 - \gamma \varepsilon \left(1 - \frac{\delta C_k}{2C_D}\right)}}.$$
 (10)

If taking $\delta = 0$ and $\gamma = 1$ and considering the definition of ϵ , Eq. (10) is reduced to

$$V_{max} = \frac{V_{EMPI}}{\sqrt{1-\varepsilon}} = \sqrt{\frac{T_s}{T_0}} V_{EMPI}. \tag{11}$$

- 247 This is actually the MPI with the DH effect included derived by BE98. In deriving (11),
- 248 BE98 assumed all the work done by surface friction being converted to DH. Since $T_s/T_0 \approx$
- 249 1.5 in the tropics, the DH leads to an increase of the EMPI (without the DH included) by
- roughly 22.5%. If taking $\delta = \gamma = 1$, Eq. (10) is reduced to

$$V_{max} = \frac{V_{EMPI}}{\sqrt{1 - \varepsilon \left(1 - \frac{C_k}{2C_D}\right)}}.$$
 (12)

This was also obtained by Edwards (2019), who assumed that the warming of the atmospheric surface layer due to DH would reduce the surface heat flux or alternatively the

heat flux is explained as the total energy flux, which includes both heat flux and kinetic
energy flux at the air-sea interface, where the kinetic energy of the ocean current is too small
compared to the kinetic energy of the air motion in the atmospheric surface layer. Consistent
with that in Edwards (2019), the reduction of surface heat flux due to the inclusion of DH
reduces the increase of the EMPI due to DH predicted by BE98. For the reasonable ratio of
$C_k/C_D \approx 0.5$, Eq. (12) predicts an increase of the EMPI without DH by roughly 15.5% ⁴ . This
means that the warming in the atmospheric surface layer due to DH reduces the increase of
the MPI with the inclusion of DH by 7% compared to that without considering the surface
layer warming effect. Note that an increase of 15.5% of the EMPI due to DH is closer to that
from previous full-physics numerical simulations (Zhang and Altshuler 1999; Jin et al. 2007;
Zeng et al. 2010; Fox and Judt (2018).

Finally, in nature, part of the work done by surface friction can be transferred to the ocean surface waves and ocean mixing layer (Kieu 2015). In this case, γ in Eq. (10) would be less than 1. If we consider $\gamma = 80\%$ and $\delta = 1$ in Eq. (10), we can get an increase of the EMPI by 11.8%. Therefore, a conservative estimate of the MPI increase due to the inclusion of DH could be between 10%~15%. Note that since the theoretical TC PIR roughly increases with the square of the MPI (Emanuel 2017b, Wang et al. 2021a, b), This implies that the inclusion of DH can lead to an increase of the PIR by 21%~32%. We will show in section 3 that the inclusion of DH may lead to more increase in the PIR for more intense TCs. This suggests that with global warming we may experience not only more intense TCs but also more rapid intensification of intense TCs.

3. Contribution of DH to the intensity-dependence of TC intensification

a. Some idealized calculations

⁴Note that we mentioned earlier that Edwards (2019) estimated an increase of the EMPI by 16.6% due to the inclusion of DH with the suppression of surface heat flux considered. The difference here is due to a slightly large ratio C_k/C_D of 0.5 instead of 0.4 used in Edwards. Nevertheless, the difference of 1.1% is within the uncertainty of the drag and exchange coefficients in nature.

277 To calculate the PIR and show the contribution of DH to the intensity-dependence of the theoretical PIR, the parameter A in Eq. (8) should be determined first. Wang (2021a) 278 parameterized A as a function of relative intensity, $\left(\frac{V_m}{V_{EMPl}}\right)^n$, with the power n (=3/2) being 279 280 calibrated based on idealized full-physics numerical simulations, and later being 281 verified/confirmed using the best track data for TCs over the North Atlantic, eastern and 282 western North Pacific (Xu and Wang 2022). Note that since the steady-state intensity based 283 on Eq. (10) (with DH) is always larger than the EMPI in Eq. (9) as discussed above, a natural modification is to replace V_{EMPI} with the steady-state intensity V_{max} discussed in section 2. 284 285 However, this replacement can substantially reduce A and thus the intensification rate for TCs at relatively weak intensity stage because of the reduced relative intensity and the power 3/2 286 287 in the definition of A. Since DH is not expected to affect the dynamical efficiency of the Carnot heat engine or the extent to which the M and s surfaces are congruent (Wang et al. 288 289 2021a, b), the replacement of the original V_{EMPI} by V_{max} could underestimate the TC PIR for relatively weak TCs. To avoid this problem, we use the same parameterization for A as in 290 291 Wang et al. (2021a) but with the relative intensity redefined using an intensity dependent 292 MPI (V_{maxt}) with DH included at the current TC intensity, namely

$$V_{maxt} = \sqrt{V_{EMPI}^2 + \gamma A \varepsilon \left(1 - \frac{\delta c_k}{2c_D}\right) V_m^2},\tag{13}$$

and we then have

301

302

303

304

305

306

$$A = \left(\frac{V_m}{V_{maxt}}\right)^{3/2}.\tag{14}$$

Since V_{maxt} is a function of A, Eqs. (13) and (14) can be solved iteratively (often three iterations are accurate enough). We can see from Eq. (13) that V_{maxt} is close to V_{EMPI} at the weak stage of the TC because DH is relatively small, but increases as the TC intensifies. Once the TC reaches its corresponding V_{max} in Eq. (10) discussed in section 2, A approache

Once the TC reaches its corresponding V_{max} in Eq. (10) discussed in section 2, A approaches 1.0 and the PIR becomes zero, and the TC reaches its steady stage.

To demonstrate the contribution of DH to the intensity dependence of TC PIR, we performed some idealized calculations and compared results from various assumptions as mentioned in section 2. For a direct comparison with results discussed in Wang et al. (2021a), we used the same values as those in Wang et al. (2021a) for our simple calculations. We take $\alpha = 0.75$, $C_D = 2.4 \times 10^{-3}$, and h = 2000m as in Wang et al. (2021a), and $\epsilon = 1/3$. Note that the thermodynamic efficiency may vary with different oceanic and atmospheric

thermodynamic conditions, which is ignored for our simple calculations here. Figure 1 shows the PIRs as a function of V_{EMPI} and V_m/V_{EMPI} for four situations, namely $\delta = \gamma = 0$; $\delta = 0$, $\gamma = 1$; $\delta = \gamma = 1$; and $\delta = 1$, $\gamma = 0.8$. We can see that without DH, the maximum PIR (MPIR) for a given V_{EMPI} appears at around the relative intensity of 0.56 (Fig. 1a). With the DH included but with the suppression of DH to surface heat flux ignored, the PIR reaches a maximum at around the relative intensity of 0.74 (Fig. 1b). In this case, the inclusion of the suppression of DH to surface heat flux shifts the maximum PIR to the relative intensity of 0.7 (Fig. 1c). If only 80% of the work done by surface friction becomes DH to warm the atmospheric surface layer, the maximum PIR would occur at the relative intensity of about 0.68 (Fig. 1d). Note that the relative intensity here is defined as the ratio of the TC intensity to the corresponding EMPI without the DH (V_{EMPI}). If the relative intensity is defined as the ratio of the TC intensity to the corresponding steady-state intensity (V_{max}) , the maximum PIR without the DH included would still occur at the relative intensity of 0.56, while that with the DH included would occur at the relative intensity of 0.60–0.61. This means that DH contributes to a shift of the maximum PIR towards the larger relative intensity side with the degree depending on the definition of relative intensity.

307

308

309

310

311

312

313

314

315

316

317

318

319

320

321

322

323

324

325

326

327

328

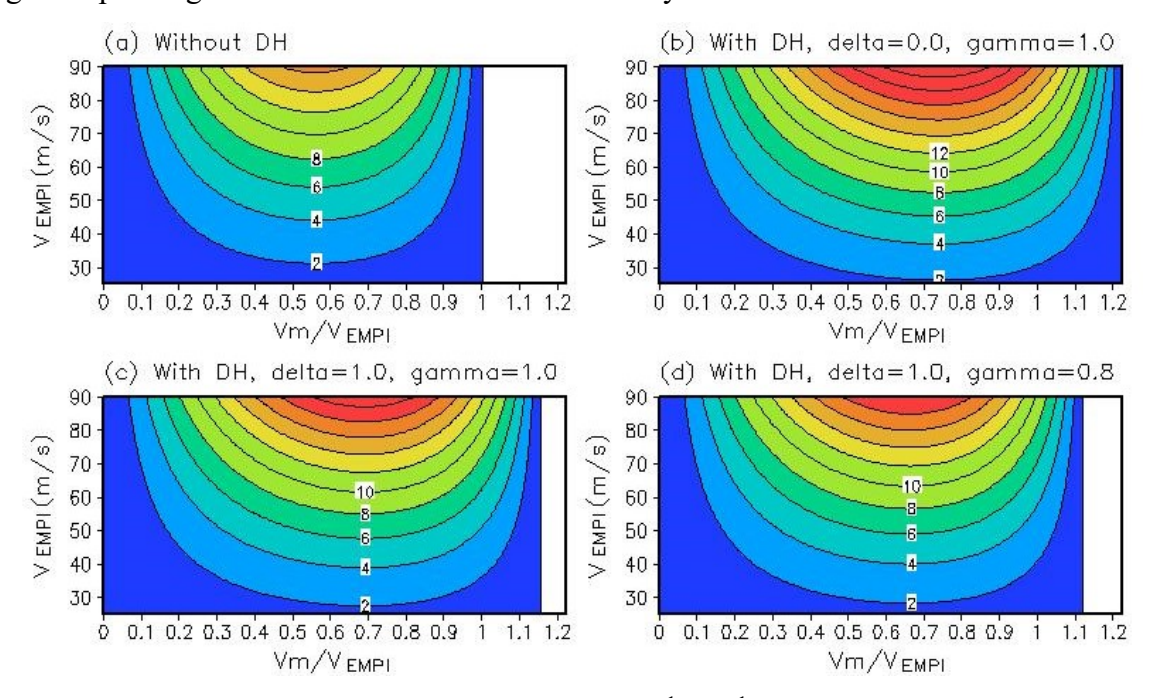


Figure 1. The calculated intensification rates [m s⁻¹(6h)⁻¹] as a function of the EMPI without the DH included (V_{EMPI} , m s⁻¹) and the corresponding relative intensity (defined as the ratio of TC intensity V_m to the corresponding V_{EMPI}) using Eq. (8) for (a) without DH, $\delta = \gamma = 0$; (b) with DH, $\delta = 0$, $\gamma = 1$; (c) with DH, $\delta = \gamma = 1$; (d) with DH, $\delta = 1$, $\gamma = 0.8$. In these calculations, we simply used $C_k/C_D=0.5$, $C_D=2.4\times10^{-3}$, $\varepsilon = 1/3$.

Figure 2 compares the PIRs as a function of relative intensity for $V_{EMPl}=55 \text{ m s}^{-1}$ and $V_{EMPl}=75 \text{ m s}^{-1}$ in the four situations as shown in Fig. 1. In addition to the contribution to a shift towards the larger relative intensity side, DH also contributes to the larger maximum PIR. For example, for the case of $V_{EMPl}=75 \text{ m s}^{-1}$, with DH but with the suppression of DH to surface heat flux ignored, the maximum PIR increases by about 39%; with the suppression of DH to surface heat flux, the maximum PIR increases by about 23%, while if only 80% of the work done by surface friction becomes DH to warm the atmospheric surface layer, the maximum PIR increases by 20%. We will show in the next subsection, the observed maximum intensification rate can be as large as $16 \text{ m s}^{-1}(6h)^{-1}$, which is considerably larger than the theoretical maximum PIR without the inclusion of DH. Therefore, it is necessary to include DH in estimating TC MPI and the maximum PIR.

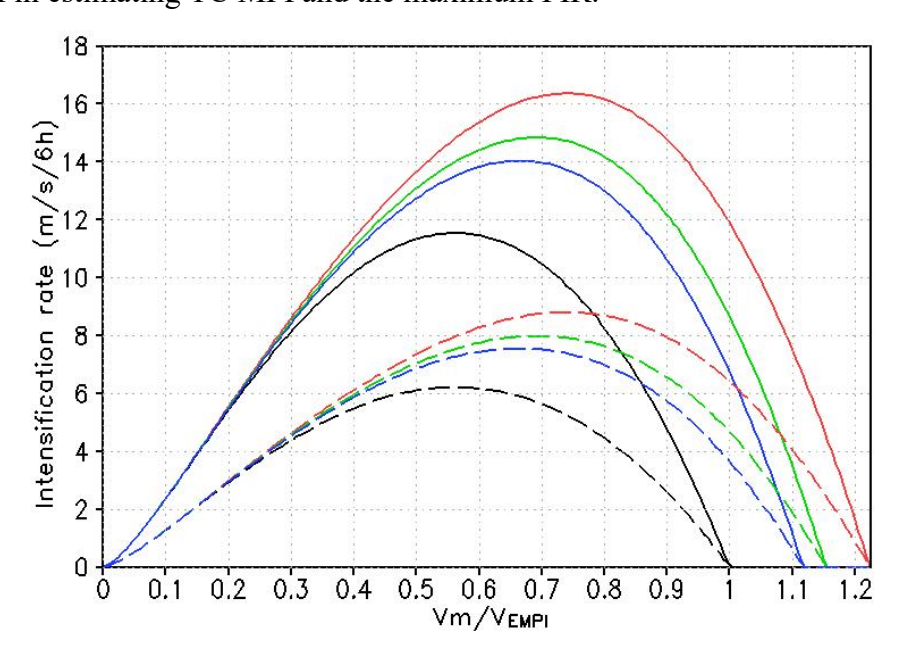


Figure 2. The intensification rates [m s⁻¹(6h)⁻¹] as a function of the relative intensity defined as the ratio of the intensity V_m to the corresponding EMPI without the DH included (V_{EMPI}) for V_{EMPI} =55 m s⁻¹ (dashed) and V_{EMPI} =75 m s⁻¹ (solid) in four situations: without DH ($\delta = \gamma = 0$, black); with DH and $\delta = 0$, $\gamma = 1$ (red); with DH and $\delta = \gamma = 1$ (green); with DH and $\delta = 1$, $\gamma = 0.8$ (blue). The same parameters and constants as used in Fig. 1 are used here.

It is also our interest to examine the time evolution of TC intensity obtained by time integration of Eq. (8) with and without the DH included. Here only results with $\delta = 1$, $\gamma = 0.8$ are considered for the case with DH because this is a reasonable scenario as argued in several previous studies (Kieu 2015; Edwards 2019). Figure 3 shows examples for four

different values of V_{EMPI} , namely 35, 50, 65, and 80 m s⁻¹, respectively. Consistent with the results discussed above and shown in Figs. 1 and 2, with DH the TC intensifies with a larger intensification rate and reaches a higher steady-state intensity. The increase in intensification rate is more significant in the second half of the intensification stage. This is mainly because DH increases with the cube of the near-surface wind speed. As predicted by Eq. (10), the steady-state intensity increases by 11-12% compared with that without the effect of DH included. Since the parameters used in our calculations are conservative as mentioned above, the results demonstrate that the contribution by DH to TC intensification and maximum intensity should be considered in both theoretical studies and numerical models used for TC intensity forecasts.

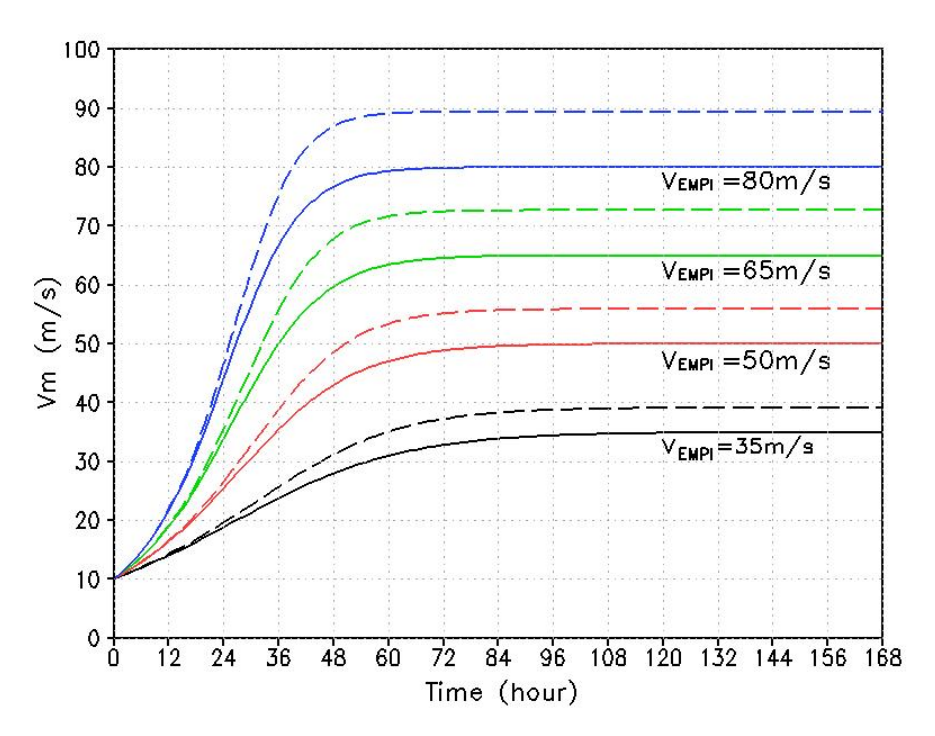


Figure 3. Time evolution of the TC intensity (V_m , m s⁻¹) obtained by the time integration of Eq. (8) for four EMPI values without the DH included (V_{EMPI} , m s⁻¹) of 35 m s⁻¹ (black), 50 m s⁻¹ (red), 65 m s⁻¹ (green), and 80 m s⁻¹ (blue) with solid for the solutions without DH and dashed for the solutions with DH and $\delta = 1$, $\gamma = 0.8$. The initial TC intensity is 10 m s⁻¹, using $\alpha = 0.75$, h = 2000 m, and $C_D = 2.4 \times 10^{-3}$.

b. Comparison with the best-track TC data

Now we compare the theoretical PIR with the observed intensification rate of TCs based on the statistical hurricane intensity prediction scheme (SHIPS) dataset (DeMaria and Kaplan 1999; Knaff et al. 2005; updated on April 3, 2020). The best-track TC data over the

371	main Northern Hemisphere basins, including all TCs over the North Atlantic, the central and
372	eastern North Pacific during 1982-2019 and those over the western North Pacific during
373	1990-2017, are considered in our comparison, as recently done in Xu and Wang (2022). The
374	variables used in our analysis from the SHIPS dataset include the 6-hourly maximum
375	sustained 10-m wind speed, and the EMPI (V_{EMPI}), and the central positions of TC centers in
376	longitude and latitude. The EMPI in the SHIPS dataset is calculated based on the standard
377	algorithm of Bister and Emanuel (2002) using the operational synoptic data derived from the
378	Climate Forecast System Reanalysis (CFSR) dataset (DeMaria and Kaplan 1999; Knaff et al.
379	2005). As in Emanuel et al. (2004) and Xu and Wang (2022), to minimize the influence of
380	TC translation on its intensity, 40% of the TC translation speed was subtracted from the
381	maximum wind speed for all TC cases in the SHIPS dataset, and the result is used as the
382	measure of TC intensity (V_m). All TC cases with 6-hourly positive intensity change and with
383	V_m greater than 17 m s ⁻¹ and being not affected by landfall are included in our analysis. In
384	addition, only TCs with tropical nature and SSTs greater than $26^\circ\!\text{C}$ are considered to exclude
385	TC cases during their extratropical transition stages.
386	In the SHIPS dataset, Xu and Wang (2022) found 166 cases out of 11758 intensifying TC
387	cases with their intensities exceeding 11% of their EMPIs, which is often termed
388	superintensity (Persing and Montgomery 2003; Wang and Xu 2010; Rousseau-Rizzi and
389	Emanuel 2019; Li et al. 2020). To avoid the theoretically estimated negative PIR due to the
390	existence of superintensity for intensifying strong TC cases, Xu and Wang (2022) simply
391	multiplied all of the SHIPS EMPIs by a factor of 1.11 to take into account of the possible
392	superintensity. Such a treatment, however, did not consider the dependence of superintensity
393	on SST recently revealed by Li et al. (2020), who found from idealized numerical simulations
394	that superintensity decreases as SST increases. Although the simple multiplication could
395	make sure there were no observed TCs with their intensity exceeding the modified MPIs, this
396	procedure may overestimate the actual MPIs and thus the PIRs for many TC cases. However,
397	we found that with a 1-2-1 (three-point) smoothing for the best-track intensity, the
398	superintensity cases are largely reduced, suggesting that part of the superintensity could be
399	due to convective variability and had little to do with the storm-scale intensity as noticed by
400	Landsea and Franklin (2013). We also found that with the inclusion of DH, almost no TC
401	cases with their intensity exceeding their corresponding MPI with DH (V_{max}). This suggests
402	that part of the superintensity in observations could be due to DH. Therefore, in our analysis,
403	we simply use the SHIPS EMPI (V_{EMPI}) without any modification. Note that although

uncertainties exist in both the estimated EMPI (Xu et al. 2019a,b) and the best-track TC intensity (Landsea and Franklin 2013), the overall results discussed below are quite reasonable and robust.

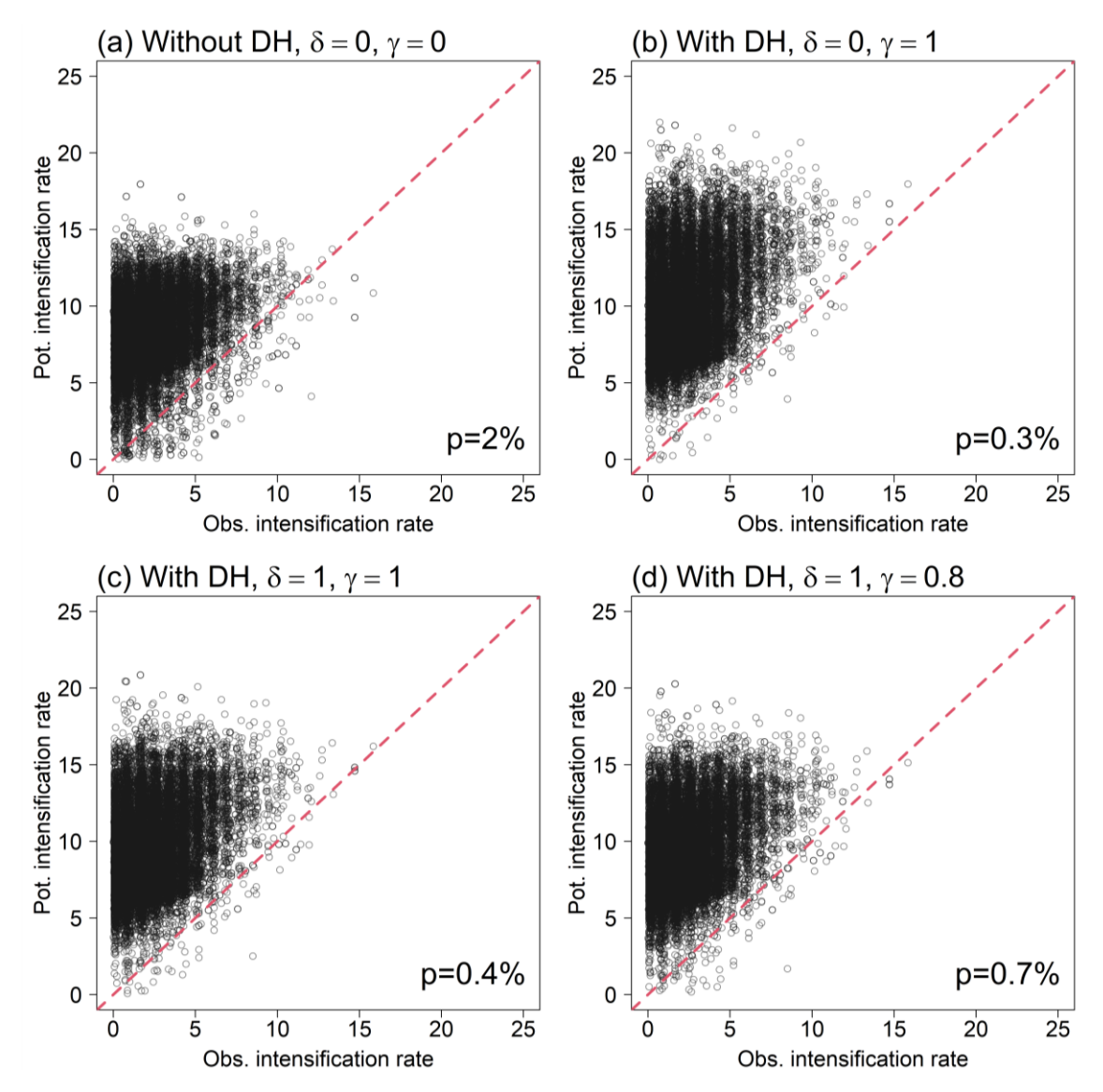


Figure 4. Scatter diagrams of the theoretically estimated potential intensification rate [PIR, m s⁻¹ (6h)⁻¹] versus the observed intensification rate [OBS, m s⁻¹ (6h)⁻¹] of all TC samples as outlined in the text for four different situations: (a) without DH ($\delta = \gamma = 0$), (b) with DH and $\delta = 0$, $\gamma = 1$, (c) with DH and $\delta = \gamma = 1$, and (d) with DH and $\delta = 1$, $\gamma = 0.8$. Red dashed lines denote y=x, and the percentage value on the right bottom of each panel gives the percentage of the case numbers with the theoretical PIR less than the observed intensification rate.

Figure 4 shows the scatter diagrams of the theoretically estimated PIRs versus the corresponding observed TC intensification rates. Four situations for the theoretically estimated PIRs are compared, including the PIR without the DH included ($\delta = \gamma = 0$), and

418 those with the DH included with $\delta = 0$, $\gamma = 1$; $\delta = \gamma = 1$; and $\delta = 1$, $\gamma = 0.8$, respectively. Note that we simply set the estimated theoretical PIR to be zero if it becomes 419 420 weakly negative (namely a few superintensity cases only) in the calculations of the PIR 421 without the DH included. Without DH (Fig. 4a), although 98% PIRs are equal to or larger 422 than the observed maximum intensification rate, there are still 2% of the theoretical PIRs are 423 smaller than the observed maximum intensification rate. The underestimation is likely to be 424 randomly distributed. With DH but with the effect of DH on surface heat flux ignored (Fig. 425 4b), the underestimation cases of the observed maximum intensification rate are largely 426 reduced to about 0.3%, but the maximum PIRs are relatively too large. With DH and the 427 effect of DH on surface heat flux included or with the work done by surface friction 428 converted to DH reduced from 100% to 80%, the results are quite similar (Figs. 4c,d). 429 Although the underestimation cases of the observed maximum intensification rate increase 430 slightly to 0.4%~0.7%, the maximum PIRs are now reduced and more comparable to the 431 observed maximum intensification rate. These results suggest that DH should be considered 432 to estimate the PIR of intensifying TCs. 433 We further compare the theoretically estimated PIR and the intensification rates of TCs 434 with their lifetime maximum intensity of category-5. This is done because most category-5 435 TCs might be closer to their MPIs (with or without DH). Figure 5 shows the scatter diagrams 436 of the theoretically estimated PIRs versus the corresponding observed TC intensification rates 437 as in Fig. 4 but for category-5 TCs only. Surprisingly, for category-5 TCs, the theoretically 438 estimated PIR without the DH included underestimates the intensification rate for 12% cases 439 (Fig. 5a), which is 6 times of that for all TC cases (Fig. 4a), suggesting that without the DH 440 included, the theoretical PIR mainly underestimates the intensification rate of strong TCs. In 441 sharp contrast, with the DH included, the theoretically estimated PIR captures the intensification rate for 98.1~99.7% TC cases. More importantly, the extremely high 442 443 intensification rates are also well reflected in the theoretically estimated PIRs with the DH 444 included (Figs. 5b,c,d). Comparing the results for all TC cases (Fig. 4) and those for 445 category-5 TC cases (Fig. 5), we can see that the overestimated theoretical PIRs occur for TC cases with relatively low intensification rates. This can be explained by three possible causes. 446 447 First, most TCs formed in deep tropics with relatively high SST and thus high MPI, which implies high PIR, but the initial TC sizes might be large and unfavorable for rapid 448 449 intensification (Xu and Wang 2015). Second, the unfavorable environmental conditions may 450 act to suppress rapid intensification of TCs. Third, most of TCs could not reach their

theoretical MPIs, the intensification of some TCs might be terminated by unfavorable environmental conditions by the TCs intensities correspond to high theoretical PIRs.

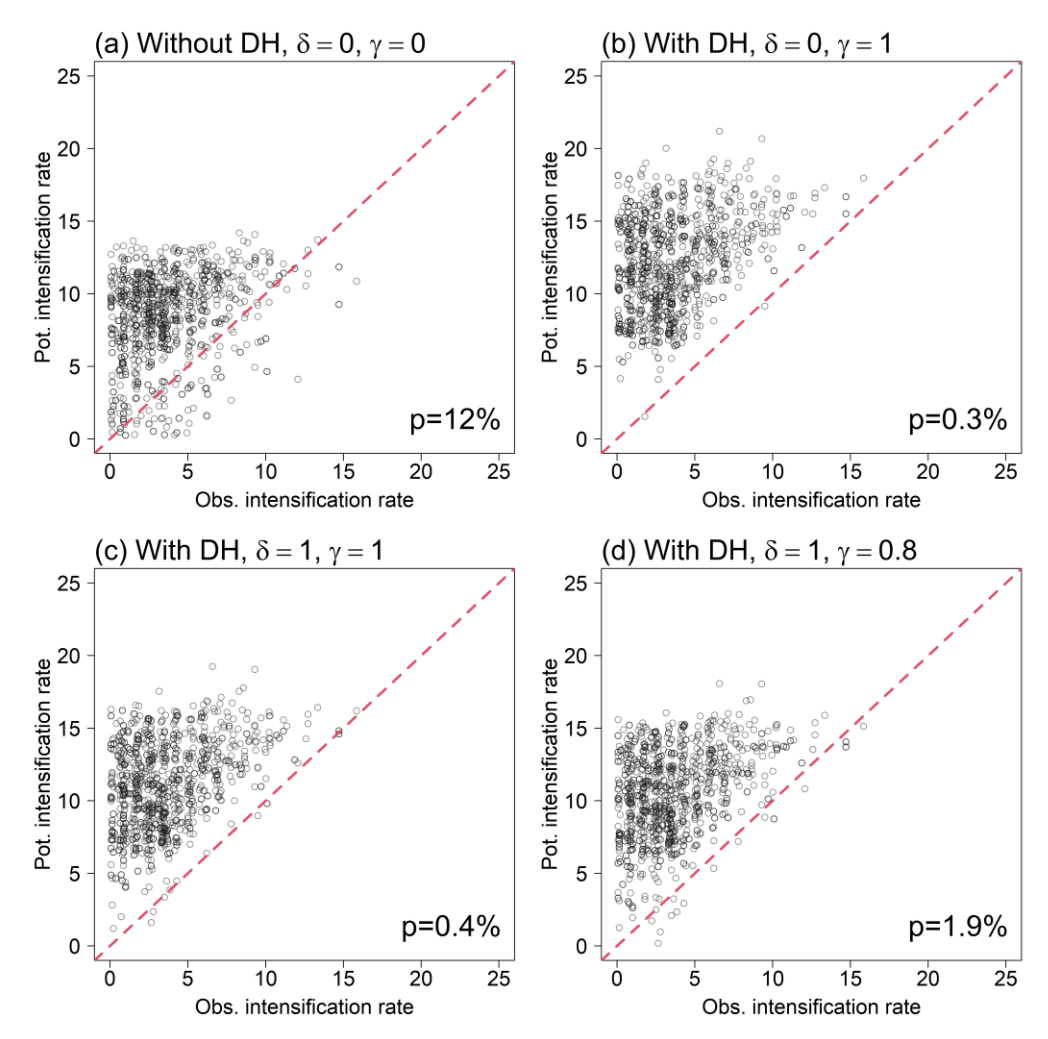


Figure 5. As in Fig. 4, but only for the observed intensification rate of TC cases with their lifetime maximum intensities that reached 5 category hurricane intensity.

It is also our interest to further examine the dependences of the theoretically estimated PIR (black dots) and the observed intensification rate (red dots) on the relative intensity defined as the ratio of the intensity to the corresponding EMPI (without DH) for category-5 TCs, with the results shown in Fig. 6. We can see that without the DH included, the high intensification rates in observed strong TCs (large relative intensity) are largely underestimated by the theoretically estimated PIRs (Fig. 6a). This is partly due to some EMPIs being smaller than the actual TC intensity, which is partly due to the existence of superintensity and partly due to the ignorance of DH in the theoretical EMPI. Such a systematic bias no longer exists with the DH included in the theoretically estimated PIRs for all three situations (Figs. 6b,c,b). Now the peak in the theoretically estimated PIRs shifts

towards the relatively high relative intensity side, consistent with the observed intensification rates. These results further confirm that DH contributes considerably to the intensity dependence of TC PIR, in particular, the PIR of strong TCs.

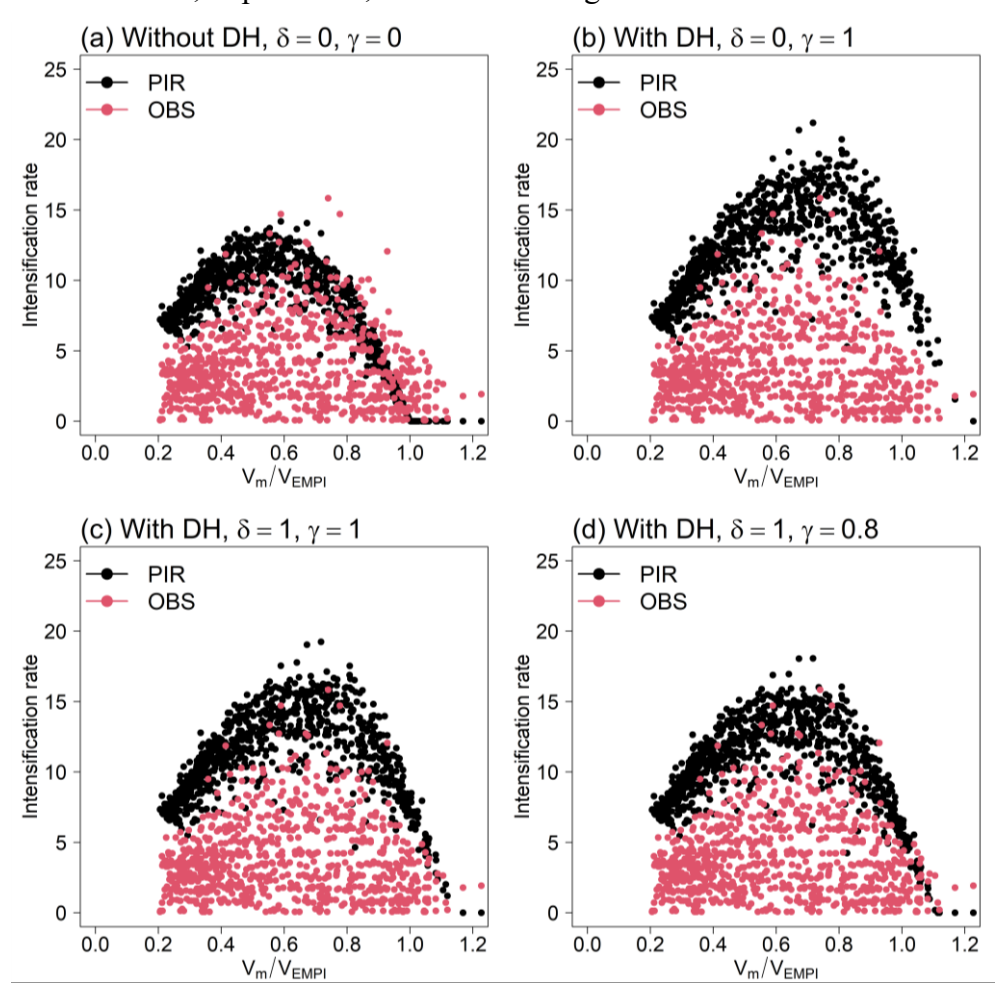


Figure 6. The Scatter diagrams of the observed intensification rate [red, m s⁻¹ (6h)⁻¹] and the theoretically estimated PIRs [black, m s⁻¹ (6h)⁻¹] against relative intensity (defined as the intensity normalized by the corresponding V_{EMPI} without DH) for TC cases with their lifetime maximum intensity that reached 5 category hurricane intensity for four different situations: (a) without DH, $\delta = \gamma = 0$; (b) with DH, $\delta = 0$, $\gamma = 1$; (c) with DH, $\delta = \gamma = 1$; (d) with DH, $\delta = 1$, $\gamma = 0.8$. We simply used $C_k/C_D=0.5$, $C_D=2.4 \times 10^{-3}$, and ε is estimated using the SST and the air temperature at 150 hPa from the SHIPS dataset.

Finally, Hurricane Patricia (2015) is considered as an example here. Patricia is the strongest hurricane in record over the eastern North Pacific (Rogers et al. 2017). It had an estimated maximum intensity of 95 m s⁻¹ while the corresponding lifetime maximum EMPI was 89.4 m s⁻¹. This means that the storm is about 6.3% stronger than its theoretical EMPI (without the DH included). Since the SST was about 32°C in the Patricia case, this could not

be explained by the superintensity because a recent modeling study indicates negligible superintensity at such a high SST (Li et al. 2020). Therefore, it is not unrealistic to assume that the excess of intensity to the theoretical EMPI (without the inclusion of DH) was due to the effect of DH. Patricia experienced a rapid weakening as a result of the suddenly increased vertical wind shear, otherwise, it might still have room to intensify. This suggests that Patricia could reach an intensity even larger than the observed maximum intensity if there was no large vertical wind shear. Patricia experienced a maximum intensification rate of 18 m s⁻¹(6h)⁻¹, which occurred when the storm intensity was 59.1 m s⁻¹, or at 66% of its theoretical EMPI (without the inclusion of DH) or 62.2% of its lifetime maximum intensity. This occurred at a much higher relative intensity than that of ~56% estimated based on the theoretical PIR without the DH included (Fig. 1a). Note that Patricia had an intensification rate of 15.4 m s⁻¹(6h)⁻¹ when its intensity was 77.1 m s⁻¹, or at ~81% of its lifetime maximum intensity. For Patricia with the SST of 32°C and in favorable environmental conditions, DH must play an important role in fueling the storm and in shifting the maximum PIR towards the high intensity side.

4. Conclusions

The viscous dissipation of kinetic energy due to surface friction can be considered as an internal heat source, often termed dissipative heating (DH), to TC intensification and maintenance. Previous studies have demonstrated that DH can significantly contribute to the MPI a TC can achieve given favorable environmental thermodynamic conditions. Since DH is a function of the near-surface wind speed and thus TC intensity, in this study, we have examined the contribution by DH to the intensity dependence of TC potential intensification rate (PIR), which is defined as the possible intensification rate a perfect TC can reach under all favorable environmental dynamic and thermodynamic conditions. We have included the effects of DH on the atmospheric surface layer (BE98; Edwards 2019) on TC potential intensification rate in a recently developed time-dependent theory of TC intensification (Wang et al. 2021a). We have shown that with the inclusion of DH, the theory predicts a shift of the maximum PIR towards the high relative intensity side. This suggests that DH can increase the PIR of strong TCs and thus contribute to the time dependence of TC PIR. The theoretical PIRs with DH are compared with the observed intensification rates of TCs based on the SHIPS dataset (DeMaria and Kaplan 1999; Knaff et al. 2005; updated on April 3, 2020) and the best-track TC data for all TCs over the North Atlantic, the central and

514	eastern North Pacific during 1982-2019 and TCs over the western North Pacific during
515	1990-2017. Results show that the inclusion of DH improves the comparison of the
516	theoretically estimated PIR with the observed intensity dependence of TC intensification rate
517	in observations, especially for strong TCs, compared with the comparison without the
518	inclusion of DH as recently done in Xu and Wang (2022). Our results thus demonstrate that
519	DH does not only contribute to the maximum possible intensity of TCs, but also contributes
520	considerably to the intensity dependence of TC PIR. Particularly, DH may considerably
521	enhance the PIR of strong TCs.
522	Considering the projected increase in TC MPI under global warming, the theory indicates
523	that as the climate continues to warm, TCs may intensify more rapidly because of the
524	increased PIR. Namely, with global warming we may experience not only more intense TCs
525	but also more rapid intensification of intense TCs. Since rapid intensification is still
526	challenging to operational TC intensity forecasting, our results imply that global warming
527	may make the TC intensity forecasting more difficult. In addition, the threats to the coastal
528	populations by landfalling TCs may increase if they intensify more rapidly just before they
529	make landfall.
530	Finally, although uncertainties in accurately estimating or calculating DH exist, results
531	from this study strongly suggest that DH should be considered in the numerical models used
532	to simulate and predict TCs, as advocated by BE98. In addition, DH may also reduce the
533	weakening rate of strong TCs (Fei et al. 2020). Therefore, future studies to evaluate and
534	improve the representation of DH in numerical models used for TC forecasts should be
535	conducted. This is particularly important to the forecasts of intensity change of strong TCs.
536	Acknowledgments.
537	The authors are grateful to Prof. Kerry Emanuel for clarification of the effect of
538	isothermal expansion on the EMPI and two other anonymous reviewers for constructive
539	review comments. This study was supported in part by the NSF grant AGS-1834300 and in
540	part by the National Natural Science Foundation of China under grants 41730960, 41875057
541	and the National Key R&D Program of China under grant 2017YFC1501602.
542	Data Availability Statement.
543	The SHIPS data are downloaded from the website https://rammb.cira.colostate.edu/
544	research/tropical_cyclones/ships/ developmental_data.asp.

546 REFERENCES

- Bister, M., and K. A. Emanuel, 2002: Low frequency variability of tropical cyclone potential
- intensity. 1. Interannual to interdecadal variability. J. Geophys. Res. Atmos., 107, 4801,
- 549 https://doi.org/10.1029/2001JD000776.
- Bister, M., and K. A. Emanuel, 1998: Dissipative heating and hurricane intensity. *Meteor*.
- 551 Atmos. Phys. **50**, 233–240, https://doi.org/10.1007/BF01030791.
- Bister, M., and K. A. Emanuel, 2011: Comment on Makarieva et al. 'A critique of some
- modern applications of the Carnot heat engine concept: the dissipative heat engine cannot
- exist'. *Proc. R. Soc. A* **467**, 1–6, https://doi.org/10.1098/rspa.2010.0087.
- Bryan, G. H., and J. M. Fritsch, 2002: A benchmark simulation for moist nonhydrostatic
- numerical model. *Mon. Wea. Rev.*, **130**, 2917–2928, https://doi.org/10.1175/1520-
- 557 0493(2002)130<2917:ABSFMN>2.0.CO;2.
- Bryan G. H., and R. Rotunno, 2009: Evaluation of an analytical model for the maximum
- intensity of tropical cyclones. J. Atmos. Sci., 66, 3042–3060,
- 560 https://doi.org/10.1175/2009JAS3038.1.
- De la Cruz, B. J., L. K. Shay, J. B. Wadler, and J. E. Rubzin, 2021: On the hyperbolicity of
- the bulk air—sea heat flux functions: Insights into the efficiency of air—sea moisture
- disequilibrium for tropical cyclone intensification. *Mon. Wea. Rev.*, **149**, 1517–1534,
- 564 https://doi.org/10.1175/MWR-D-20-0324.1.
- 565 Cheng, X. P., J. F. Fei, X. G. Huang, and J. Zheng, 2012: Effects of sea spray evaporation
- and dissipative heating on intensity and structure of tropical cyclone. Adv. Atmos. Sci., 29,
- 567 810–822. https://doi.org/10.1007/s00376-012-1082-3.
- 568 Edwards, J. M. 2019: Sensible heat fluxes in the nearly neutral boundary layer: The impact of
- frictional heating within the surface layer. *J. Atmos. Sci.*, **76**, 1039-1053.
- 570 https://doi.org/10.1175/JAS-D-18-0158.1.
- 571 Emanuel, K. A., 1986: An air-sea interaction theory for tropical cyclones. Part I: Steady-state
- 572 maintenance. J. Atmos. Sci., 43, 585–605, https://doi.org/10.1175/1520-
- 573 0469(1986)043<0585:AASITF>2.0.CO;2.
- 574 Emanuel, K. A., 1988: The maximum intensity of hurricanes. J. Atmos. Sic., 45, 1143–1155,
- 575 https://doi.org/10.1175/1520-0469(1988)045<1143:TMIOH>2.0.CO;2.

- 576 Emanuel, K. A., 1995: The behavior of a simple hurricane model using a convective scheme
- based on subcloud-layer entropy equilibrium. J. Atmos. Sci., **52**, 3960–3968,
- 578 https://doi.org/10.1175/1520-0469(1995)052<3960:TBOASH>2.0.CO;2.
- Emanuel, K. A., 1997: Some aspects of hurricane inner-core dynamics and energetics. J.
- 580 Atmos. Sci., **54**, 1014–1026, https://doi.org/10.1175/1520-
- 581 0469(1997)054<1014:SAOHIC>2.0.CO;2.
- 582 Emanuel, K. A., 2012: Self-stratification of tropical cyclone outflow: Part II: Implications to
- storm intensification. J. Atmos. Sci., **69**, 988–996, https://doi.org/10.1175/JAS-D-11-
- 584 0177.1.
- 585 Emanuel, K., 2017a: A fast intensity simulator for tropical cyclone risk analysis. *Nat.*
- 586 *Hazards*, **88**, 779–796, https://doi.org/10.1007/s11069-017-2890-7.
- 587 Emanuel, K. A., 2017b: Will global warming make hurricane forecasting more difficult?
- 588 Bull. Amer. Meteor. Soc., 98, 495–501, https://doi.org/10.1175/BAMS-D-16-0134.1.
- Emanuel, K. A., C. DesAutels, C. Holloway, and R. Korty, 2004: Environmental control of
- tropical cyclone intensity. J. Atmos. Sci., 61, 843–858, https://doi.org/10.1175/1520-
- 591 0469(2004)061,0843:ECOTCI.2.0.CO;2.
- Emanuel, K. and F. Zhang, 2017: The role of inner-core moisture in tropical cyclone
- 593 predictability and practical forecast skill. J. Atmos. Sci., 74, 2315–2324,
- 594 https://doi.org/10.1175/JAS-D-17-0008.1.
- 595 Fei, R., J. Xu, Y. Wang, and C. Yang, 2020: Factors affecting the weakening rate of tropical
- 596 cyclones over the western North Pacific. Mon. Wea. Rev., 148, 3693–3712,
- 597 https://doi.org/MWR-D-19-0356.1.
- 598 Fox, K. R., and F. Judt, 2018: A numerical study on the extreme intensification of Hurricane
- 599 Patricia (2015). Wea. Forecasting, **33**, 989–999, https://doi.org/10.1175/WAF-D-17-
- 600 0101.1.
- Frisius, T., 2006: Surface-flux-induced tropical cyclogenesis within an axisymmetric
- atmospheric balanced model. Q. J. Roy. Meteor. Soc., 132, 2603–2623,
- 603 https://doi.org/10.1256/qj.06.03.
- 604 Gray, S., and G. Craig, 1998: A simple theoretical model for the intensification of tropical
- 605 cyclones and polar lows. *Q. J. Roy. Meteor. Soc.*, **124**, 919–947,

- 606 https://doi.org/10.1002/qj.49712454713.
- Jin, Y., W. T. Thompson, S. Wang, and C. Liou, 2007: A numerical study of the effect of
- dissipative heating on tropical cyclone intensity. Wea. Forecasting, 22, 950–966,
- 609 https://doi.org/10.1175/WAF1028.1.
- Kieu, C. 2015: Revisiting dissipative heating in tropical cyclone maximum potential
- 611 intensity. Quart. J. Roy. Meteor. Soc., 141, 2497–2504, https://doi.org/10.1002/qj.2534.
- Knaff, J.A., C.R. Sampson, and M. DeMaria, 2005: An operational statistical typhoon
- intensity prediction scheme for the western North Pacific. Wea. Forecasting, 20, 688–
- 614 699, https://doi.org/10.1175/WAF863.1.
- 615 Li, T.-H., and Y. Wang, 2021: The role of boundary layer dynamics in tropical cyclone
- intensification. Part I: Sensitivity to surface drag coefficient. J. Meteor. Soc. Japan, 99,
- 617 537–554, https://doi.org/10.2151/jmsj.2021-027.
- 618 Li, Y., Y. Wang, Y. Lin, and R. Fei, 2020: Dependence of superintensity of tropical cyclones
- on SST in axisymmetric numerical simulations. *Mon. Wea. Rev.*, **148**, 4767–4781,
- 620 https://doi.org/10.1175/MWR-D-20-0141.1.
- 621 Li, Y., Y. Wang, Y. Lin, and X. Wang, 2021: Why does rapid contraction of the radius of
- maximum wind precede rapid intensification in tropical cyclones? J. Atmos. Sci., 78,
- 623 3441–3453, https://doi.org/10.1175/JAS-D-21-0129.1.
- Makarieva, A. M., V. G. Gorshkov, B.-L. Li, and A. D. Nobre, 2010: A critique of some
- modern applications of the Carnot heat engine concept: the dissipative heat engine cannot
- exist. *Proc. R. Soc. A* **466**, 1893–1902. https://doi.org/10.1098/rspa.2009.0581.
- Ming, J., and J. A. Zhang, 2018: Direct measurements of momentum flux and dissipative
- heating in the surface layer of tropical cyclones during landfalls. J. Geophys. Res. –
- 629 Atmos., **123**, 4926–4938, https://doi.org/10.1029/2017JD028076.
- Peng, K., R. Rotunno, and G. H. Bryan, 2018: Evaluation of a time-dependent model for the
- intensification of tropical cyclones. J. Atmos. Sci., 75, 2125–2138,
- https://doi.org/10.1175/JAS-D-17-0382.1.
- Rogers, R. F., S. Aberson, M. M. Bell, D. J. Cecil, J. D. Doyle, T. B. Kimberlain, J.
- Morgerman, L. K. Shay, and C. Velden, 2017: Rewriting the tropical record books. *Bull*.
- 635 Ameri. Meteorol. Soc., 98, 2092–2112, https://doi.org/10.1175/BAMS-D-16-0039.1.

- Rotunno, R., and G. H. Bryan, 2012: Effects of parameterized diffusion on simulated
- hurricanes. J. Atmos. Sci., **69**, 2284–2299, https://doi.org/10.1175/JAS-D-11-0204.1.
- Rousseau-Rizzi, R., and K. Emanuel, 2019: An evaluation of hurricane superintensity in
- Axisymmetric Numerical Models. J. Atmos. Sci., 76, 1697–1706,
- 640 https://doi.org/10.1175/JAS-D-18-0238.1.
- Smith, A. W., B. K. Haus, and J. A. Zhang, 2019: Stability and sea state as limiting
- conditions for TKE dissipation and dissipative heating. J. Atmos. Sci., 76, 689-706,
- 643 https://doi.our/10.1175/JAS-D-18-0142.1
- Vickery, P. J., P. F. Skerlj, A. C. Steckley, and L. A. Twisdale, 2000: Hurricane wind field
- model for use in hurricane simulations. J. Struct. Eng., 126, 1203–1221,
- 646 https://doi.org/10.1061/(ASCE)0733-9445(2000)126:10(1203).
- Wang, Y., 2001: An explicit simulation of tropical cyclones with a triply nested movable
- mesh primitive equation model—TCM3. Part I: Description of the model and control
- experiment. Mon. Wea. Rev., 129, 1370–1394, https://doi.org/10.1175/1520-
- 650 0493(2001)129<1370:AESOTC>2.0.CO;2.
- Wang, Y., and J. Xu., 2010: Energy production, frictional dissipation, and maximum intensity
- of a numerically simulated tropical cyclone. J. Atmos. Sci., 67, 97–116,
- 653 https://doi.org/10.1175/2009JAS3143.1.
- Wang, Y., Y. Li, and J. Xu, 2021a: A new time-dependent theory of tropical cyclone
- intensification. J. Atmos. Sci., 78, 3855–3865, https://doi.org/10.1075/JAS-D-21-0169.1.
- Wang, Y., Y. Li, J. Xu, Z.-M. Tan, and Y. Lin, 2021b: The intensity-dependence of tropical
- 657 cyclone intensification rate in a simplified energetically based dynamical system model.
- 658 *J. Atmos. Sci.*, **78**, 2033–2045, https://doi.org/10.1175/JAS-D-20-0393.1.
- 659 Xu, J., and Y. Wang, 2015: A statistical analysis on the dependence of tropical cyclone
- intensification rate on the storm intensity and size in the North Atlantic. Wea.
- *Forecasting*, **30**, 692–701, https://doi.org/10.1175/WAF-D-14-00141.1.
- Ku, J., Y. Wang, and Z.-M. Tan, 2016: The relationship between sea surface temperature and
- 663 maximum potential intensification rate of tropical cyclones over the North Atlantic. J.
- Atmos. Sci., 73, 4979–4988, https://doi.org/10.1175/JAS-D-16-0164.1.
- Ku, J., and Y. Wang, 2018: Dependence of tropical cyclone intensification rate on sea surface
- temperature, storm intensity and size in the western North Pacific. Wea. Forecasting, 33,

- 523–537, https://doi.org/10.1175/WAF-D-17-0095.1.
- Xu, J., Y. Wang, and C. Yang, 2019a: Factors affecting the variability of maximum potential
- intensity (MPI) of tropical cyclones over the North Atlantic. J. Geophys. Res.: Atmos.,
- 670 **124**, 6654–6668. https://doi.org/10.1029/2019JD030283.
- Xu, J., Y. Wang, and C. Yang, 2019b: Interbasin differences in the median and variability of
- tropical cyclone MPI in the northern hemisphere. J. Geophys. Res.: Atmos., 124, 13,714—
- 673 13,730, https://doi.org/10.1029/2019JD031588.
- Xu, J., and Y. Wang, 2022: Potential intensification rate of tropical cyclones in a simplified
- 675 energetically based dynamical system model: An observational analysis. J. Atmos. Sci.,
- **79**, 1045–1055, https://doi.org/10.1175/JAS-D-21-0217.1.
- Zeng, Z.-H., Y. Wang, Y.-H. Duan, L.-S. Chen, and Z.-Q. Gao, 2010: On sea surface
- 678 roughness parameterization and its effect on tropical cyclone structure and intensity. Adv.
- 679 Atmos. Sci., 27, 337–355, https://doi.org/10.1007/s00376-009-8209-1.
- Zhang, C.-X., Y. Wang, and M. Xue, 2020: Evaluation of an *E*-ε and three other boundary
- layer parameterization schemes in the WRF model over the Southeast Pacific and the
- Southern Great Plains, Mon. Wea. Rev., 148, 1121–1145, https://doi.org/10.1175/MWR-
- 683 D-19-0084.1.
- Zhang, D.-L., and E. Altshuler, 1999: The effects of dissipative heating on hurricane
- intensity. Mon. Wea. Rev., 127, 3032–3038, https://doi.org/10.1175/1520-
- 686 0493(1999)127,3032:TEODHO.2.0.CO;2.
- Kenney, J. A., and F. D. Marks, 2015: Effects of horizontal diffusion on tropical cyclone
- 688 intensity change and structure in idealized three-dimensional numerical simulations. *Mon.*
- 689 Wea. Rev., 143, 3981–3995, https://doi.org/10.1175/MWR-D-14-00341.1
- Karaman English Englis
- observations in the hurricane boundary layer. *J. Atmos. Sci.*, **67**, 1853–1862,
- 692 https://doi.org/10.1175/2010JAS3397.1.
- Zhou, K., Q.-Q. Li, J. Tang, 2022: Estimation of dissipative heating properties above the
- internal boundary layer in landfalling typhoons using multi-layer tour observations.
- 695 Frontiers Earth Sci., 10:833994, https://doi.org/10.3389/feart.2022.833994.